

Journal of Materials Chemistry C

Accepted Manuscript



This is an *Accepted Manuscript*, which has been through the Royal Society of Chemistry peer review process and has been accepted for publication.

Accepted Manuscripts are published online shortly after acceptance, before technical editing, formatting and proof reading. Using this free service, authors can make their results available to the community, in citable form, before we publish the edited article. We will replace this *Accepted Manuscript* with the edited and formatted *Advance Article* as soon as it is available.

You can find more information about *Accepted Manuscripts* in the [Information for Authors](#).

Please note that technical editing may introduce minor changes to the text and/or graphics, which may alter content. The journal's standard [Terms & Conditions](#) and the [Ethical guidelines](#) still apply. In no event shall the Royal Society of Chemistry be held responsible for any errors or omissions in this *Accepted Manuscript* or any consequences arising from the use of any information it contains.

Morphological control and plasmonic tuning of nanoporous gold disks by surface modifications

Jianbo Zeng,^a Fusheng Zhao,^a Ming Li,^a Chien-Hung Li,^b T. Randall Lee,^b and Wei-Chuan Shih^{*a,c}

^aDepartment of Electrical and Computer Engineering

^bDepartment of Chemistry

^cDepartment of Biomedical Engineering

University of Houston, 4800 Calhoun Road, Houston, TX 77204, USA

* Corresponding Author, Email: wshih@uh.edu Phone: +1 713-743-4454; Fax: 713-743-4444

Abstract

We report a surface modification protocol to control nanoporous gold (NPG) disk morphology and tune its plasmonic resonance. Enlarged pore size up to ~20 nm within 60 s dealloying time has been achieved by adsorbing halides onto alloy surfaces in between two dealloying steps. In addition, plasmonic resonance has been significantly redshifted for up to ~258 nm by the surface modification. Furthermore, with the enlarged pore size, small gold nanoparticles have been effectively loaded into the pores to enhance the performance of surface-enhanced Raman scattering (SERS) due to hot spot formation between the original nanoporous network and loaded nanoparticles.

Introduction

Plasmonic metal nanostructures exhibit wide applications ranging from optics and biomedicine to catalysis.^{1,2,3,4} Their plasmonic properties such as surface plasmon resonance (SPR) and localized surface plasmon resonance (LSPR) is significantly dependent on the composition, shape and size.⁵ Moreover, the plasmon resonance bands can be tuned based on refractive index changes through organic solvents,⁶ adsorption of alkanethiolate surfactants⁷ and voltage-controlled tuning liquid crystals.^{8,9,10,11} Bulk nanoporous gold (NPG) as a nanostructured semi-infinite thin film material has recently attracted intense attention due to the unique 3-dimensional bicontinuous nanostructures with large surface area, high catalytic activity and tunable plasmonic resonance.^{12,13,14} Porous nanostructures are typically formed during the dealloying process by either concentrated nitric acid or electrochemistry. Thus, the pore and ligament size can be controlled by varying experimental parameters, including alloy atomic compositions, dealloying time, thermal annealing temperatures, electrolytes and critical potential.^{14, 15,16,17, 18,19} Recently, lithographically patterned nanoporous gold disks (NPGDs) in disk shape or nanoparticles demonstrated that unique plasmonic nanomaterials with tunable plasmonics, 3-dimensional plasmonic hot spot distribution, large surface area, and large surface-enhanced Raman scattering (SERS) enhancement factor.^{20,21,22,23} Taking advantage of the high-density hot spots in NPGDs, we have developed several applications such as ultrasensitive DNA hybridization monitoring at the level of individual molecules,²⁴ and integrated microfluidic SERS sensor for label-free biomolecular sensing.²⁵

Pore size control and plasmonic tuning in NPGDs is challenging using existing techniques that are effective for NPG thin films. The primary reason is that NPGDs are individual particles with no structural constraints at lengthscale larger than a few hundred nanometers. NPGDs are allowed to significantly shrink by as much as 33-37% during the formation of the internal nanoporous structures,²³ leading to the ineffectiveness to enlarge pore size simply by prolonged dealloying or pre-dealloying thermal annealing. To circumvent, our previous attempts included post-dealloying thermal annealing and laser rapid thermal annealing.^{26,27} Although these techniques are more effective, they require additional processing steps and additional apparatus. More importantly, these techniques usually cause undesirable pore coalescence and pore count reduction, which could lead to smaller total surface area.

In this paper, we have taken a surface modification approach using halide compounds such as KI and KBr, inspired by Dursun and Ankaç's work on forming NPG thin films by electrochemical corrosion. Briefly, Dursun *et al.* showed that halide-containing electrolytes could reduce the critical potential to control the nanoporous structures in electrochemical corrosion.¹⁸ Ankaç *et al.* further elucidated surface morphology control of nanoporous structures by the addition of halides into H₂SO₄ electrolytes.¹⁹ Compared to their works, our approach would provide the flexibility of working with both conductive and nonconductive substrates.

To summarize our findings, the pre-adsorbed halide ions at the surface result in size growth of both the pore and ligament, where the size is strongly dependent on the halide ion concentrations. Redshift of the major plasmonic extinction band up to ~258 nm has been observed due to morphological changes, which is different from blueshift caused by

timed dealloying or post-annealing thermal annealing. In addition, we have applied surface modification to produce large pore sizes for loading small gold nanoparticles into pores. Such pore enlargement have not been possible without significantly increasing the dealloying time. Improved performance of SERS has been observed in both halide modified and gold nanoparticles loaded NPGDs.

Materials and methods

Chemicals and materials

Nitric acid (ACS reagent, 70%), chloroform (anhydrous, $\geq 99.0\%$), sodium dodecyl sulfate, (ACS reagent, $\geq 99.0\%$), 3,3'-diethylthiatricocyanine iodide (DTTC, 99%), potassium iodide (ReagentPlus, $\geq 99.0\%$), potassium bromide (ACS reagent, $\geq 99\%$), poly(diallyldimethylammonium chloride) (PDDA, 20 wt.% in H₂O) and latex beads (polystyrene beads, 10% aqueous suspension) with mean particle sizes 460 nm were purchased from Sigma Aldrich. Polystyrene beads were purified by centrifugation at 8000 rpm before use. Ethanol (200 proof) was from Decon Laboratories, Inc. Silicon wafers were obtained from University Wafers, and coverglass (22 × 40 mm, No.1) from VWR. Ag_{82.5}Au_{17.5} and Ag₇₀Au₃₀ (atomic percentage) alloy sputtering targets was purchased from ACI Alloys, Inc. Argon gas (99.999%) was used for RF-sputter etching and protection of thermal annealing.

Fabrication of monolithic NPGDs

Detailed fabrication process was described in elsewhere of our works.²³ The as-prepared Au-Ag alloy nanoparticles were incubated with KI (or KBr) aqueous solutions for 24 hours before delloying. Finally, NPGDs were produced by dealloying Ag in 70% nitric

acid for 30 to 270 s. The sample was washed in deionized (DI) water to remove the dealloying reaction products and excess nitric acid.

Characterization.

Scanning electron microscope (SEM) images were obtained from PHILIPS FEI XL-30 FEG SEM. X-ray photoelectron spectroscopy (XPS) spectra were collected by using a PHI 5700 system equipped with a monochromatic Al K α X-ray source ($h\nu = 1486.7$ eV). A Cary 50 Scan UV-visible spectrometer and Jasco V-570 UV-Vis-NIR spectrophotometer were used to measure extinction spectra of the monolayer NPGDs on a glass coverslip (~ 1.0 mm \times 0.5 mm). The SERS spectra of DTTC were recorded by using a home-built line-scan Raman microscope (LSRM).²⁸ An automated image curvature correction algorithm was employed with 5th-order polynomial background removal.²⁸

Results and discussion

Surface modification-induced morphological changes

In order to investigate the effects of surface modification on NPGDs, I⁻ and Br⁻ ions were pre-adsorbed onto Ag_{82.5}Au_{17.5} and Ag₇₀Au₃₀ (atomic percentage) alloy nanoparticles before dealloying. SEM images of samples after dealloying are shown in Fig. 1a-f for comparison. Fig. 1a-c show 300 nm diameter NPGDs obtained from Ag_{82.5}Au_{17.5} alloy without the halide surface modification, with Br⁻, and with I⁻, respectively. Without halides (Fig. 1a), the average pore size was about 11.2 nm, and the average ligament size was about 14.3 nm. After modified with Br⁻ (Fig. 1b), the average size of pores and ligaments slightly increased to 13.4 and 17.2 nm, respectively. When the surface was treated with KI (Fig.1c), larger pores (16.8 nm) and ligaments (19.5 nm) were obtained

compared to those without modification or with KBr. The KI-induced morphological change appeared to be rougher with ligaments condensed onto gold-rich clusters to form larger units. As for NPGDs from the $\text{Ag}_{70}\text{Au}_{30}$ alloy (Fig. d-f), the average pore size increased from 8.5 to 11.9 nm with KBr modification, and to 16.4 nm with KI modification. The average ligament size corresponding to without, with KBr and KI surface modification were 12.4, 20.7 and 26.7 nm, respectively. Consistently, surface modification by pre-adsorbed halides induced an increase in the size of pores and ligaments, which could be understood by the effect of halides on critical potential. In the electrochemical corrosion process, the addition of halides to the electrolyte led to the critical potential decrease of AgAu alloys for removing Ag, e.g. significantly dropping 50% at the presence of 0.1 M KI.¹⁸ Lowered critical potential causes fast etching of Ag atoms and promotes surface diffusion of gold atoms which accelerates the size growth of the pore and ligament.^{18,19} At the electrolyte/alloy interface, halides have much stronger affinity than those of ClO_4^- and SO_4^{2-} to the metal surface, therefore, halide adsorption at the alloy surface plays a key role in the critical potential decrease. Instead of dealloying in halide-containing electrolytes, pre-adsorbed halides onto the alloy surface in pure halide aqueous solutions can be similarly understood. Concentrated nitric acid drives the fast surface diffusion due to lowered critical potential by the pre-adsorbed halides. Thus, surface modification results in similar fast growth in pore and ligament sizes within short dealloying time, and offers a facile and alternative protocol to control NPGDs morphology. In addition, it is interesting to point out that the halide-induced morphology of NPGDs obtained from $\text{Ag}_{82.5}\text{Au}_{17.5}$ alloy is slightly different from that made by $\text{Ag}_{70}\text{Au}_{30}$, e.g., in KI-induced morphology (Fig. 1c and f). As revealed by Dursun,¹⁸ the

critical potential of AuAg alloy with a lower gold atomic percentage is smaller than that of alloy possessing a higher gold atomic percentage in halide-containing electrolytes. Therefore, the alloy with a lower gold atomic percentage would experience faster surface diffusion to form nanoporous structures. In Fig. 1c, the bicontinuous network almost broke down and the ligaments grew into bead-like nanostructures due to the

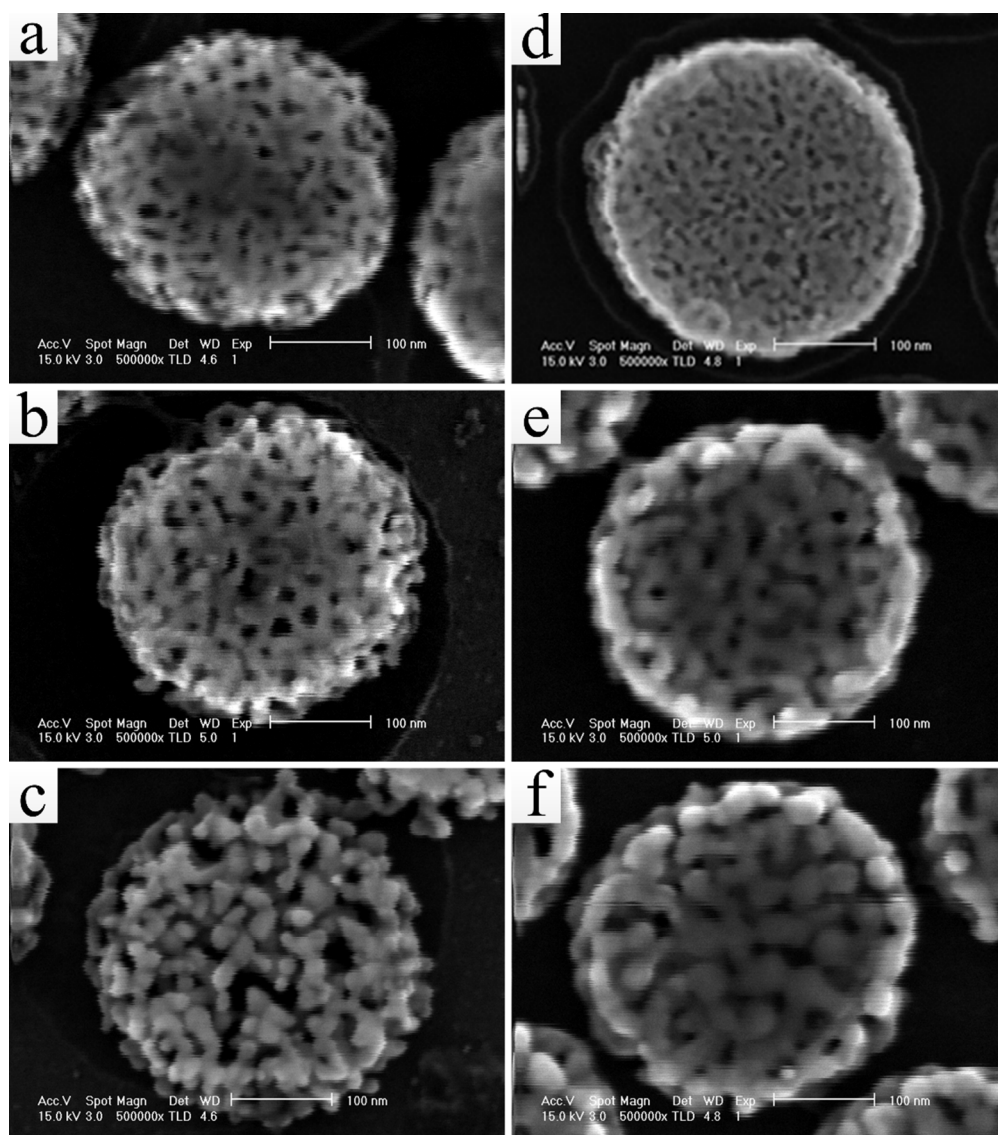


Figure 1. Ag_{82.5}Au_{17.5} alloy dealloys 30s: (a) without halides, (b) with 0.1 M KBr and (c) with 0.1 M KI. Ag₇₀Au₃₀ alloy dealloys 60s: (d) without halides, (e) with 0.1 M KBr and (f) with 0.1 M KI. SEM scale bar: 100 nm.

accelerated dealloying rate, while NPGD in Fig. 1f still keeps its bicontinuous network with relatively large ligaments. Our observations are consistent with Dursun's work.

Surface modification-induced plasmonic changes

Fig. 2 shows the morphology-dependent plasmonic resonance of surface modified NPGDs obtained from different alloy atomic compositions. In Fig. 2a, NPGDs without halides exhibited an extinction band at 990 nm, which has been interpreted as the in-plane resonance of the disk (i.e., Disk LSPR).²³ The in-plane resonance band redshifted ~68 nm for the KBr modified sample, and ~258 nm for the KI modified sample. NPGDs obtained from Ag₇₀Au₃₀ alloy also exhibited similar trend of redshift (Fig. 2b): ~42 nm for KBr modification and additional ~147 nm for KI modification. Smaller redshifts were observed from Ag₇₀Au₃₀ alloy compared to those from Ag_{82.5}Au_{17.5} alloy. In our previous work,²⁶ we observed that the in-plane resonance band blueshifted due to increased pore and ligament size, interpreted as decreased plasmonic coupling between the in-plane Disk LSPR and NPG LSPR. However, surface modification-induced NPGDs exhibit redshifts even though seemingly similar morphological coarsening were observed.

To further investigate why the LSPR band shifted into the opposite direction after halide surface modifications, we compared the extinction spectra of naked NPGDs without surface modification and NPGDs with post-dealloying adsorbed halides. As shown in Fig. S1, after adsorbing halides, the extinction band of NPGDs significantly redshifted ~88 nm. The observed redshifts were caused by adsorbed halides on the

surface that resulted in refractive index changes in the local environment near the nanoporous structures. To further support this interpretation, we have applied X-ray photoelectron spectroscopy (XPS) to quantitatively characterize the composition of adsorbed I⁻ before (Fig. S2a) and after dealloying (Fig. S2b). The 3d peaks of I⁻ are shown in Fig. S2. The binding energy of 3d_{5/2} slightly shifted to lower binding energy (~619.0 eV) due to adsorbed I⁻ on metal surfaces.

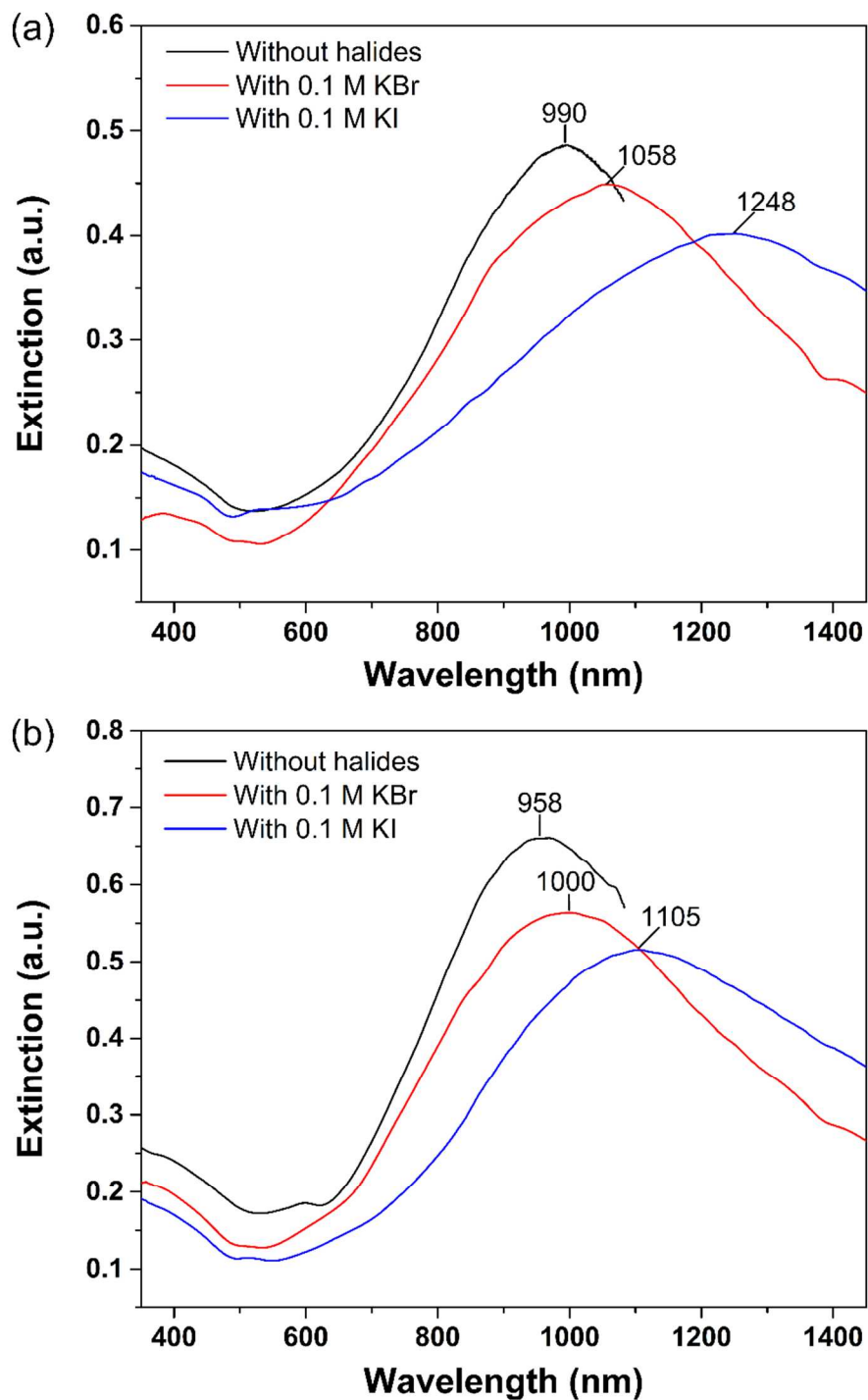


Figure 2. Extinction spectra of NPGDs obtained from different alloys: (a) $\text{Ag}_{82.5}\text{Au}_{17.5}$ alloy, and (b) $\text{Ag}_{70}\text{Au}_{30}$ alloy. Black lines are without halides. Red and blue lines are with 0.1 M KBr and KI, respectively.

XPS surface compositional analysis revealed 14.9% adsorbed I⁻ on the surface before dealloying, while the iodide composition dropped to 7.8% after dealloying. Apparently, there were still a significant amount of I⁻ residues on NPGDs which was responsible for the refractive index changes and the subsequent plasmonic redshifts.

Effects of halide concentration

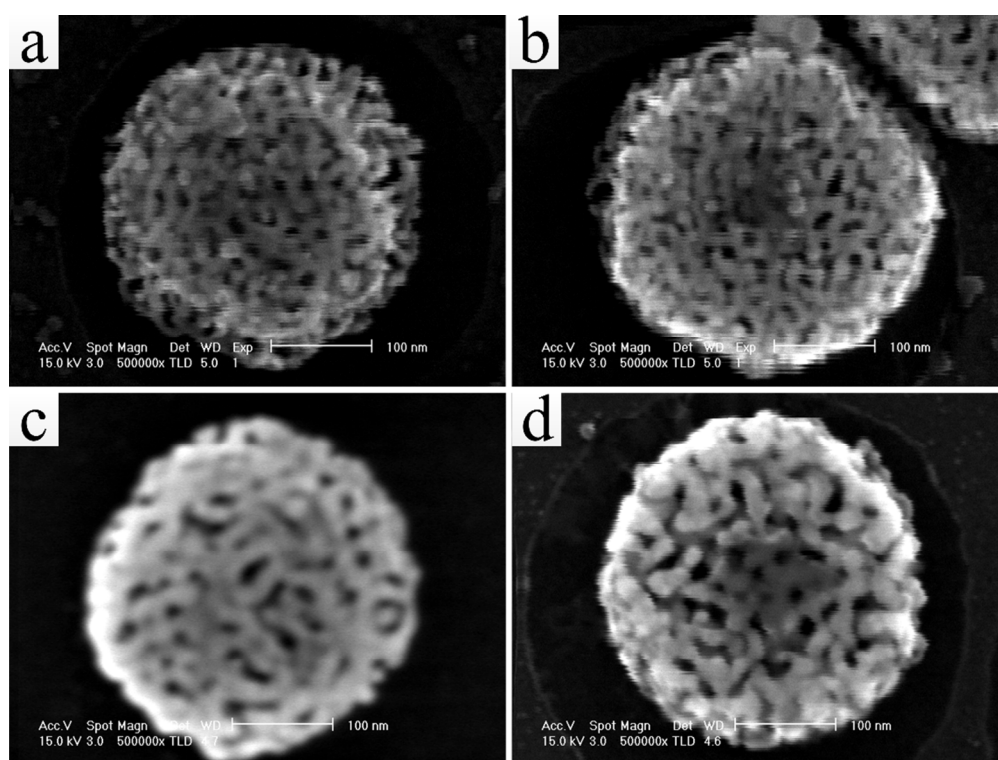


Figure 3. NPGDs obtained from $\text{Ag}_{82.5}\text{Au}_{17.5}$ alloy after incubating in different concentrations of halides: (a) 1 mM and (b) 10 mM KBr; (c) 1 mM and (d) 10 mM KI. Dealloying 30 s. SEM scale bar: 100 nm.

To further investigate the effects of halide concentration on the induced morphology, we incubated $\text{Ag}_{82.5}\text{Au}_{17.5}$ alloy nanoparticles in different concentrations of halides (1 and 10

mM) before dealloying. Fig. 3 shows SEM images of NPGDs dealloyed at 30 s after surface modification with KBr and KI. Under the low concentrations of KBr (Fig. 3a and 3b), the average pore sizes of NPGDs were 11.3 and 11.8 nm for 1 and 10 mM KBr, respectively. The corresponding average ligament size were 14.4 and 14.8 nm. For low concentrations KI (Fig. 3c and d), the average pore size was 12.4 nm with 1 mM KI and 13.5 nm with the higher concentration at 10 mM. The average ligament size increases from 16.6 to 21.1 nm. Apparently, lower halide concentration resulted in less pore and ligament enlargement. Fig. 4 shows extinction spectra of as-prepared NPGDs by using different halide concentrations. In Fig. 4a, the extinction band blueshifted ~ 48 nm as the KBr concentration increased from 1 to 10 mM, and it further blueshifted ~ 24 nm by using 100 mM KBr. Similar blueshifts were also observed by increasing the concentration of KI (Fig. 4b), where the extinction band blueshifted ~ 72 nm when the KI concentration increased from 1 to 100 mM. As mentioned earlier, we found that the increased pore and ligament size results in blueshifts due to the decrease of the plasmonic coupling between the in-plane Disk LSPR and NPG LSPR.²⁶ Since NPGDs were modified by the same halide and likely similar amounts of residues after dealloying, the nanoporous structure such as the size of pores and ligaments should play a key role in the plasmonic resonance. Therefore, the blueshift of extinction bands of halide-induced NPGDs can be understood by the decrease of the plasmonic coupling since their pore size increased.

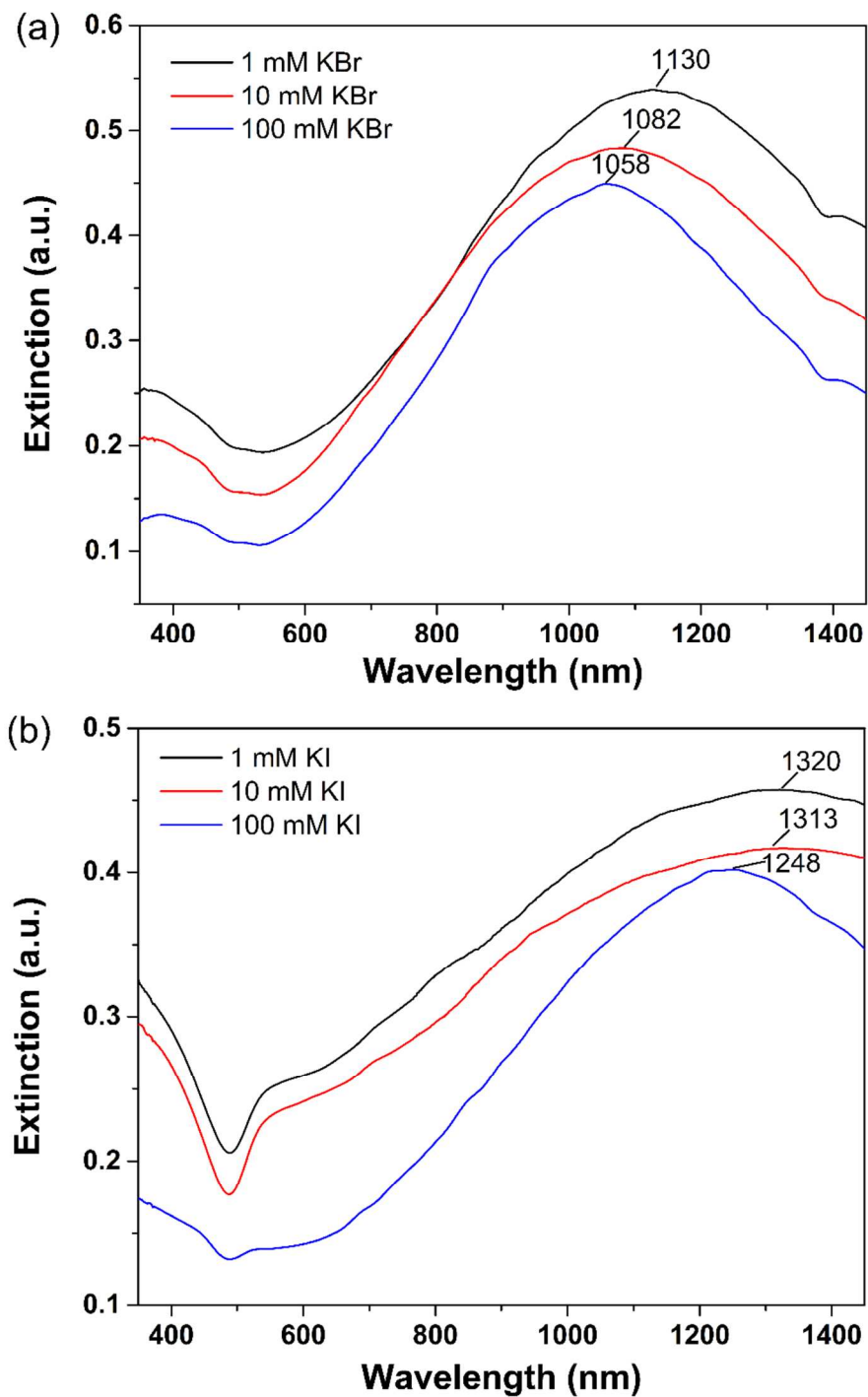


Figure 4. Extinction spectra of NPGDs obtained from $\text{Ag}_{82.5}\text{Au}_{17.5}$ alloy. Incubated in different concentrations: (a) 1, 10 and 100 mM KBr; (b) 1, 10 and 100 mM KI.

Applications of surface modification-induced morphology and plasmonics in NPGDs

The simple surface modification protocol described in this paper offers an alternative way to control the morphology of NPGDs. Herein, we used this method to produce enlarged pore size for loading small gold nanoparticles for potential applications such as surface-enhanced Raman scattering (SERS). Instead of directly dealloying halide-modified alloy nanoparticles, we employed a two-step method to enlarge the pore size: alloy nanoparticles were first dealloyed without pre-adsorbed halides to achieve nanoporous structures and then halides were adsorbed, followed by a second dealloying step. The rationale behind this approach is that the opened pores after the first dealloying step can

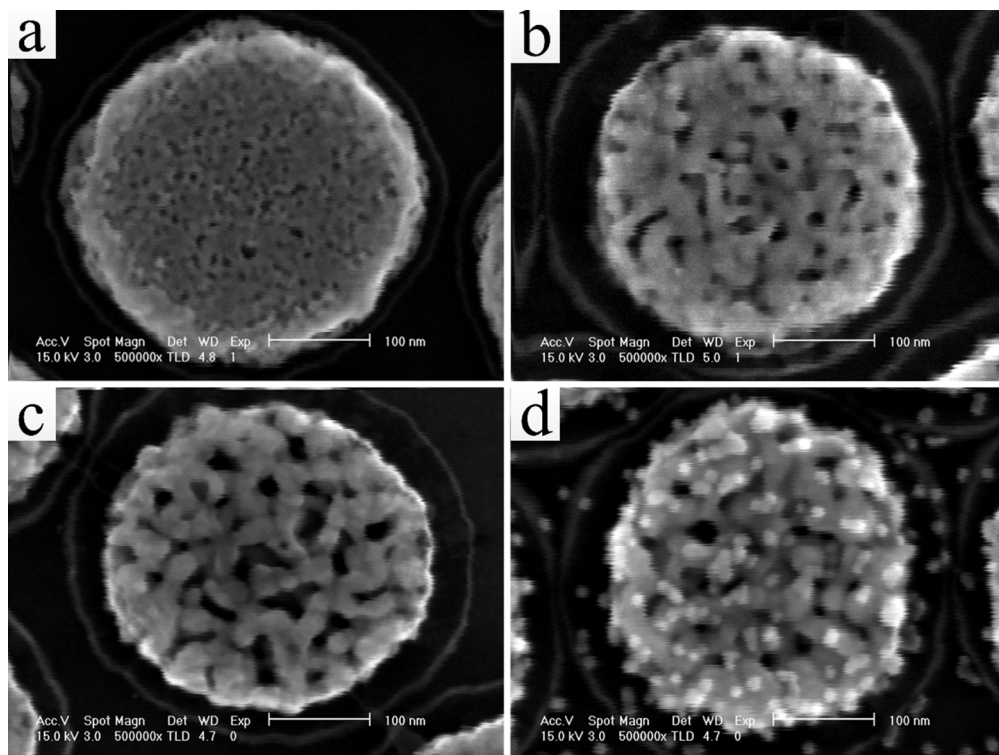


Figure 5. SEM images of as-dealloyed NPGDs from Ag₇₀Au₃₀ alloy. (a) Dealloying 30 s and (b) dealloying 270 s without halides. (c) As-dealloyed NPGDs at 30 s incubated with 0.1 M KI for 24 h first, then further dealloyed 30 s again. (d) Attached ~12 nm gold nanoparticles on NPGDs of (c).

adsorb halides not only on outside surfaces but also inside surfaces of nanoporous structure which is expected to further accelerate the growth rate of the pores. This approach created a “discrete” version of the electrochemical dealloying with the presence of halides in the electrolyte for continuous supply as dealloying progresses. Herein, we take NPGDs obtained from Ag₇₀Au₃₀ alloy as an example for applications. Fig. 5a shows as-dealloyed NPGDs at 30 s with an average pore size ~7.8 nm. For comparison, the dealloying time was increased to 270 s and the average pore size increased to ~12.2 nm (Fig. 5b). Fig. 5c shows NPGDs were prepared with the two-step method, where as-dealloyed NPGDs at 30 s were first incubated with 0.1 M KI and then further dealloyed for 30 s. The average pore size increases to ~20 nm which is much larger than that of NPGDs dealloyed at 270 s (Fig. 5b), as well as NPGDs directly obtained from surface modified Ag₇₀Au₃₀ alloy (Fig. 1f). NPGDs with large pores can be used to load small gold nanoparticles prepared, e.g., by Turkevich protocol.^{29,30,31} To demonstrate this, NPGDs were first made positively charged by a coating of poly(diallyldimethylammonium chloride) (PDDA),^{32,33} followed by incubating with negatively charged gold nanoparticles (~12 nm) for loading. As shown in Fig. 5d, small gold nanoparticles were successfully loaded into pores, and some of them attached on ligaments.

To explore surface modification-induced NPGDs for SERS application, diethylthiatricarbocyanine (DTTC) dye molecule was used as the SERS marker to

compare performance. Fig. 6a shows DTTC SERS spectra on NPGDs without halides (black trace), KI-induced NPGDs (red trace), and KI-induced NPGDs loaded with small gold nanoparticles (blue trace). SERS intensity variation of the peak at 1150 cm^{-1} with standard deviation was also shown in Fig. 6b. Interestingly, SERS intensity of DTTC on KI-induced

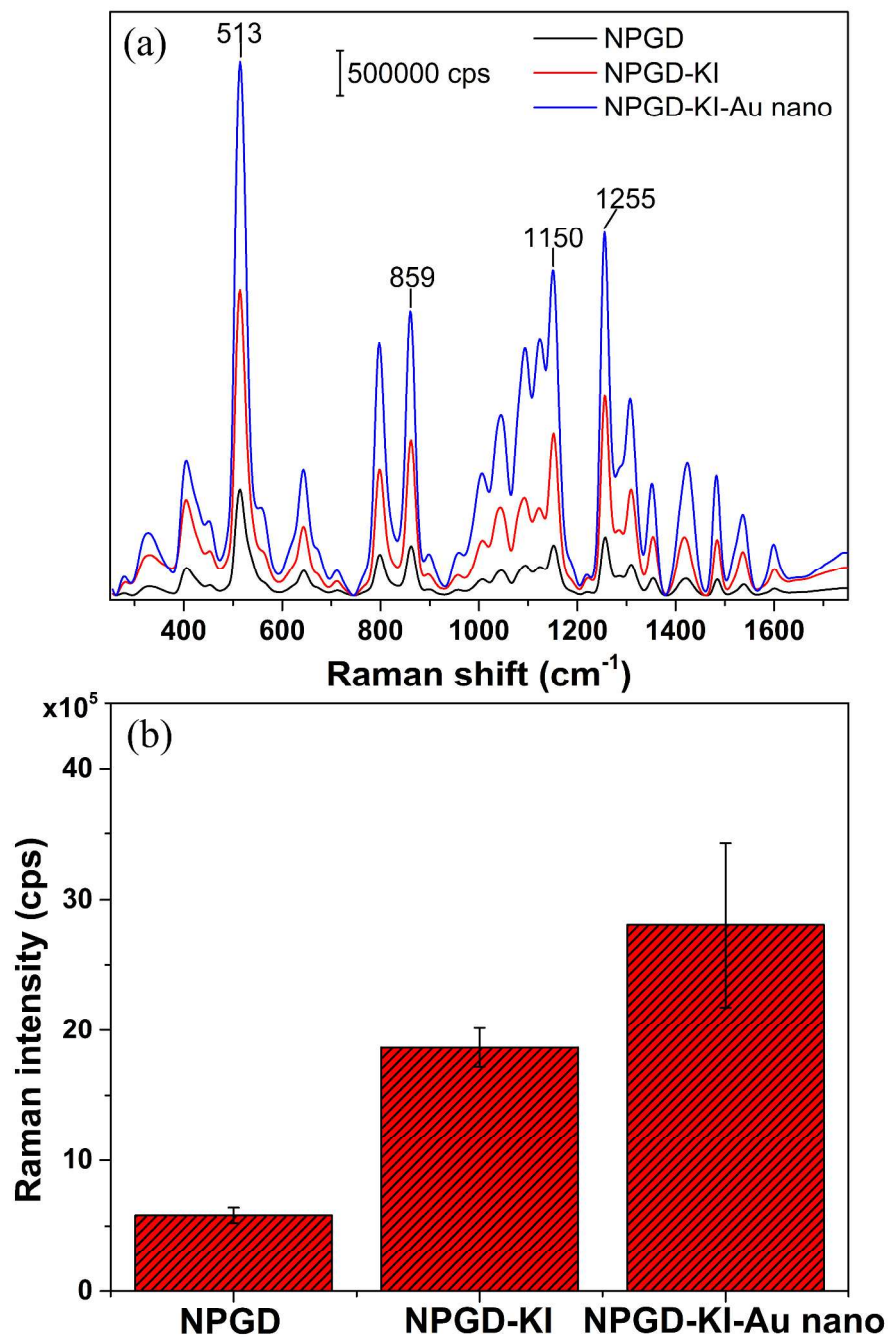


Figure 6. (a) DTTC SERS spectra at NPGDs without halides (black line), KI-induced NPGDs, and KI-induced NPGDs loaded with small gold nanoparticles (blue line). (b) Raman intensity at the peak at 1150 cm^{-1} with standard deviation.

NPGDs increased ~ 3 folds compared to NPGDs without KI. It is noted that for NPGDs without halides, the growth of pore and ligament sizes by increasing dealloying time

resulted in blueshifts of plasmonic bands.²⁶ Therefore, the LSPR peak matches the average of the laser excitation and the SERS wavelengths.²⁶ However, in the presence of KI, the LSPR peak of KI-induced NPGDs significantly redshifts to ~ 1200 nm as mentioned earlier, which is far away from the average of the laser excitation and Raman wavelengths. Hence, more enhancement increase could be obtained using a laser wavelength near the plasmonic peak. Moreover, the rough structure caused by KI might have played an important role for the additional enhancement. The enhancement performance was further improved by loading small gold nanoparticles onto NPGDs. As shown in Fig. 6b, SERS intensity was ~ 5.6 times larger than that of NPGDs without KI modification. The interaction between nanopores and nanoparticles, as well as the adjacent nanoparticles, corresponds to the strong enhancement, which agrees with previous work.³¹ It will be of interest to further explore biosensing based on halide-induced NPGDs loaded with small gold or other metallic nanoparticles. We are currently pursuing these directions in our laboratory.

Conclusions

In summary, we have developed a surface modification strategy to control NPGD morphology and tune its plasmonic resonance. A simple protocol has been employed to effectively produce enlarged pores that are otherwise challenging to achieve in NPGDs. We have found that the NPGDs fabricated with pre-adsorbed halides exhibited significant plasmonic redshift for up to ~ 258 nm. We have demonstrated that the enlarged pores can be employed to harbor small gold nanoparticles. Further studies have revealed that SERS performance of KI-modified NPGDs and KI-modified NPGDs loaded with small gold nanoparticles increased by ~ 3 and 5.6 folds, respectively. Therefore, they could be applicable to surface-enhanced spectroscopy, as well as molecular sensing.

Acknowledgements

W.C.S. acknowledges the National Science Foundation (NSF) CAREER Award (CBET-1151154), National Aeronautics and Space Administration (NASA) Early Career Faculty Grant (NNX12AQ44G) and a grant from Gulf of Mexico Research Initiative (GoMRI-030).

Notes and References

Electronic Supplementary Information (ESI) available: extinction spectra of NPGDs adsorbed halides and XPS analysis of iodide. See DOI: 10.1039/b000000x/

1. J. R. Krenn, *Nat Mater*, 2003, 2, 210-211.
2. G. A. Sotiriou, *Wiley Interdisciplinary Reviews: Nanomedicine and Nanobiotechnology*, 2013, 5, 19-30.
3. F. Pincella, K. Isozaki and K. Miki, *Light Sci Appl*, 2014, 3, e133.
4. P. Swarnakar, S. R. Kanel, D. Nepal, Y. Jiang, H. Jia, L. Kerr, M. N. Goltz, J. Levy and J. Rakovan, *Solar Energy*, 2013, 88, 242-249.
5. K. L. Kelly, E. Coronado, L. L. Zhao and G. C. Schatz, *The Journal of Physical Chemistry B*, 2002, 107, 668-677.
6. Y. Sun and Y. Xia, *Analytical Chemistry*, 2002, 74, 5297-5305.
7. E. M. Larsson, J. Alegret, M. Käll and D. S. Sutherland, *Nano Letters*, 2007, 7, 1256-1263.
8. Y. Wang, *Applied Physics Letters*, 1995, 67, 2759-2761.
9. P. A. Kossyrev, A. Yin, S. G. Cloutier, D. A. Cardimona, D. Huang, P. M. Alsing and J. M. Xu, *Nano Letters*, 2005, 5, 1978-1981.
10. L. De Sio, T. Placido, S. Serak, R. Comparelli, M. Tamborra, N. Tabiryan, M. L. Curri, R. Bartolino, C. Umeton and T. Bunning, *Advanced Optical Materials*, 2013, 1, 899-904.
11. L. De Sio, G. Klein, S. Serak, N. Tabiryan, A. Cunningham, C. M. Tone, F. Ciuchi, T. Burgi, C. Umeton and T. Bunning, *Journal of Materials Chemistry C*, 2013, 1, 7483-7487.
12. Arne Wittstock, Jürgen Biener, Jonah Erlebacher and M. Bäumer, *Nanoporous Gold: From an Ancient Technology to a High-Tech Material*, Royal Society of Chemistry; 2012.
13. T. Fujita, P. Guan, K. McKenna, X. Lang, A. Hirata, L. Zhang, T. Tokunaga, S. Arai, Y. Yamamoto and N. Tanaka, *Nature Materials*, 2012, 11, 775-780.
14. X. Lang, L. Qian, P. Guan, J. Zi and M. Chen, *Applied Physics Letters*, 2011, 98, 093701-093703.
15. D. Wang, R. Ji, A. Albrecht and P. Schaaf, *Beilstein Journal of Nanotechnology*, 2012, 3, 651-657.

16. G. Gupta, J. Thorp, N. Mara, A. Dattelbaum, A. Misra and S. Picraux, *Journal of Applied Physics*, 2012, 112, 094320-094327.
17. L. Qian, X. Yan, T. Fujita, A. Inoue and M. Chen, *Applied physics letters*, 2007, 90, 153120-153123.
18. A. Dursun, D. Pugh and S. Corcoran, *Journal of the Electrochemical Society*, 2003, 150, B355-B360.
19. G. N. Anka, A. Pareek, S. Cherevko, A. A. Topalov, M. Rohwerder and F. U. Renner, *Electrochimica Acta*, 2012, 85, 384-392.
20. J.-S. Wi, S. Tominaka, K. Uosaki and T. Nagao, *Physical Chemistry Chemical Physics*, 2012, 14, 9131-9136.
21. D. Wang and P. Schaaf, *Journal of Materials Chemistry*, 2012, 22, 5344-5348.
22. J. Qi, P. Motwani, M. Gheewala, C. Brennan, J. C. Wolfe and W.-C. Shih, *Nanoscale*, 2013, 5, 4105-4109.
23. F. Zhao, J. Zeng, M. M. P. Arnob, P. Sun, J. Qi, P. Motwani, M. Gheewala, C.-H. Li, A. Paterson, U. Strych, B. Raja, T. R. Lee, R. C. Willson, J. C. Wolfe and W.-C. Shih, *Nanoscale*, 2014, 6, 8199-8207.
24. J. Qi, J. Zeng, F. Zhao, S. H. Lin, B. Raja, U. Strych, R. C. Willson and W.-C. Shih, *Nanoscale*, 2014, 6, 8521-8526.
25. M. Li, F. Zhao, J. Zeng, J. Qi, J. Lu and W.-C. Shih, *Journal of biomedical optics*, 2014, 19, 111611-111611.
26. J. Zeng, F. Zhao, J. Qi, Y. Li, C.-H. Li, Y. Yao, T. R. Lee and W.-C. Shih, *RSC Advances*, 2014, 4, 36682-36688.
27. M. M. P. Arnob, F. Zhao, J. Zeng, G. Santos, M. Li and W.-C. Shih, *Nanoscale*, 2014, 6, 12470-12475.
28. J. Qi and W.-C. Shih, *Applied Optics*, 2014, 53, 2881-2885.
29. B. V. Enustun and J. Turkevich, *Journal of the American Chemical Society*, 1963, 85, 3317-3328.
30. J. Kimling, M. Maier, B. Okenve, V. Kotaidis, H. Ballot and A. Plech, *The Journal of Physical Chemistry B*, 2006, 110, 15700-15707.
31. L. Qian, B. Das, Y. Li and Z. Yang, *Journal of Materials Chemistry*, 2010, 20, 6891-6895.
32. R. G. Freeman, K. C. Grabar, K. J. Allison, R. M. Bright, J. A. Davis, A. P. Guthrie, M. B. Hommer, M. A. Jackson, P. C. Smith, D. G. Walter and M. J. Natan, *Science*, 1995, 267, 1629-1632.
33. X. Li, W. Xu, J. Zhang, H. Jia, B. Yang, B. Zhao, B. Li and Y. Ozaki, *Langmuir*, 2004, 20, 1298-1304.

TOC

